EPJ B
Condensed Matter and Complex Systems
EPJ.org
your physics journal

Eur. Phys. J. B (2012) 85: 109 DOI: 10.1140/epjb/e2012-20635-0

# Weak localization and dimensional crossover in carbon nanotube systems

M. Salvato, M. Lucci, I. Ottaviani, M. Cirillo, S. Orlanducci, F. Toschi and M.L. Terranova

EDP SCIENCES
Società Italiana di Fisica
Springer

Eur. Phys. J. B (2012) 85: 109
DOI: 10.1140/epjb/e2012-20635-0

THE EUROPEAN PHYSICAL JOURNAL B

Regular Article

# Weak localization and dimensional crossover in carbon nanotube systems

M. Salvato[1], M. Lucci[1], I. Ottaviani[1], M. Cirillo[1,a], S. Orlanducci[2], F. Toschi[2], and M.L. Terranova[2]

[1] Dipartimento di Fisica and MINAS Laboratory, Università di Roma "Tor Vergata", 00133 Roma, Italy
[2] Dipartimento di Scienze e Tecnologie Chimiche and MINAS Laboratory, Università di Roma "Tor Vergata", 00133 Roma, Italy

Received 4 May 2011 / Received in final form 3 January 2012
Published online 30 March 2012 – 

**Abstract.** We investigate the effects of magnetic and electric fields on electron wavefunction interactions in single walled carbon nanotube bundles. The magnetoresistance measurements performed at 4.2 K and the dependence of the data upon the electric field reveal good agreement with weak localization theory. An electrical field conditioned characteristic length is associated to ohmic-non ohmic transition, observed below 85 K, in current voltage characteristics. This length results equal to the average bundles diameter just at $T \cong 85$ K, indicating that 2D-3D crossover is responsible for the observed conductance transition.

Among the theories and the models [1–5] conceived to give account for experimental data in terms of electron wavefunctions properties and interactions in low-dimensional systems the weak localization (WL) theory [6] occupies a role which has been relevant and productive. WL theory has been successfully used for explaining the properties of disordered metallic [7] and semiconducting films [8] as well as aggregates of carbon nanotube bundles [9,10]. The theory assumes that inside the inelastic scattering length $L_i = (D\tau_i)^{1/2} > l_0$, where $D$ is the electrons diffusion constant, $\tau_i$ the inelastic scattering time and $l_0$ the elastic mean free path, the electrons are elastically scattered by impurities preserving the coherence of their wavefunctions along a coherence diffusion length $L_\varphi = (D\tau_\varphi)^{1/2}$ with $\tau_\varphi$ the dephasing time of the electron wavefunction. As a result of elastic scattering, electrons covering a two time reversed paths interfere with themselves giving rise to a decrease in the electrical conductivity $\sigma$. External fields and temperature affect the electron wavefunction coherence and cause a change in $\sigma$ [11]. WL theory also predicts that $\sigma$ depends on the sample dimension $d$: depending on whether the value of the ratio $d/L_\varphi$ is lower or greater than the unity, respectively 2 or 3 dimensional (2D or 3D) effects can be evidenced. In this paper we intend to demonstrate that, for a system of single walled carbon nanotubes (SWCNT), the WL theory can provide a satisfactory explanation of the effects generated by external magnetic and electric fields.

Aggregates of SWCNT bundles have been deposited in our laboratory on Si-SiO substrates and aligned along the current direction by dielectrophoresis techniques [12]. On the substrates, prior to the deposition, we patterned four gold contacts acting as current and voltages electrodes as shown in the scanning electron microscope (SEM) image of Figure 1a. The distance between the two voltage probes (the internal ones) is $l_V = 5$ $\mu$m while the distance between the two current electrodes is $l_c = 60$ $\mu$m. The average diameter of each SWCNT is $d_{SWCNT} = 1.2$ nm and the diameter of the bundles, measured by SEM is $d_B = 80 \pm 20$ nm. The SWCNT bundles had lengths ranging in the interval (1–10) $\mu$m and the SEM analysis evidenced that the bundles were indeed deposited in the form of aggregates bridging the contact pads. Three layers of bundles in the direction perpendicular to the substrate surface, corresponding to a sample thickness of approximately 250 nm, have been detected by SEM (Fig. 1b). The measurements herein reported are very typical of a set of a dozen samples that we investigated. The SWCNT network resulting by the deposition and alignment on the substrate were previously characterized by electrical measurements in a wide temperature range [13]. Moreover, Joule heating contribution due to bias current has been calculated and experimentally evaluated as negligible for all measurements presented here [13].

The temperature measurements in the range (4–300 K) were performed by thermally anchoring the samples to the cold finger of a high vacuum cryocooler while the magneto resistance ($MR$) measurements were performed keeping the samples in He liquid bath inside a cryostat equipped with a 6 T superconducting magnet. The magnetic field $B$ is oriented parallel to the substrate surface and perpendicular to the current direction. In Figure 2a we plot the normalized $MR = [R(B) - R(0)]/R(0)$ vs. $B$, where $R(B)$ and $R(0)$ are the sample resistances measured with

[a] e-mail: cirillo@roma2.infn.it

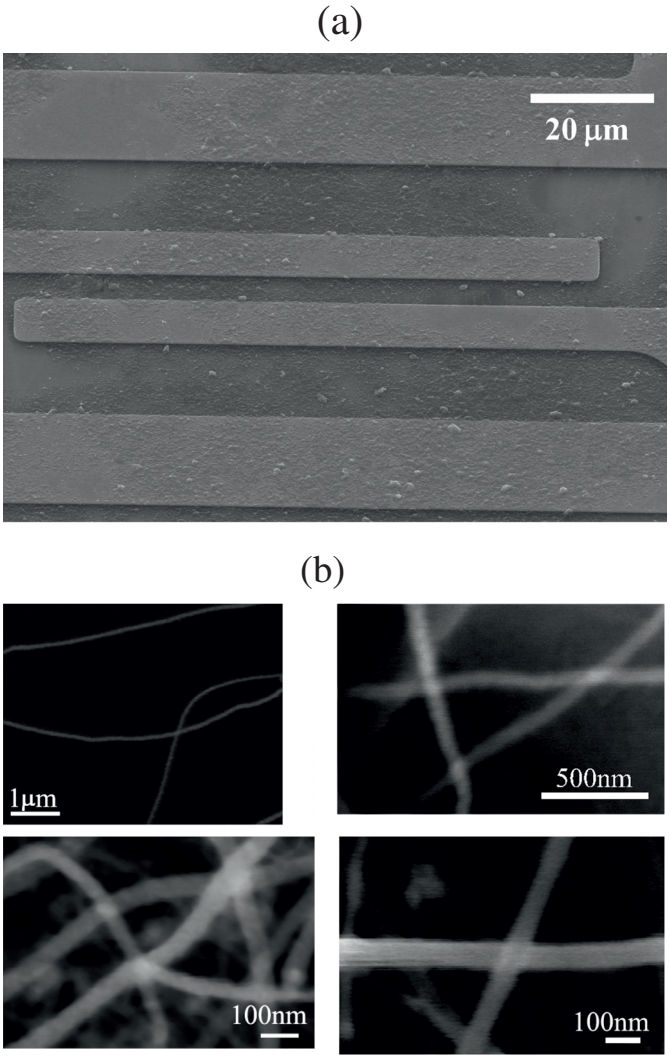


**Fig. 1.** SEM images of our samples (a) the four gold probe configuration and (b) details of our single-walled carbon nanotube (SWCNT) bundles aggregates contacting the gold electrodes: each bundle is represented by a single white filament in the photos with a diameter of the order of 100 nm. Also well visible are the junctions between the bundles.

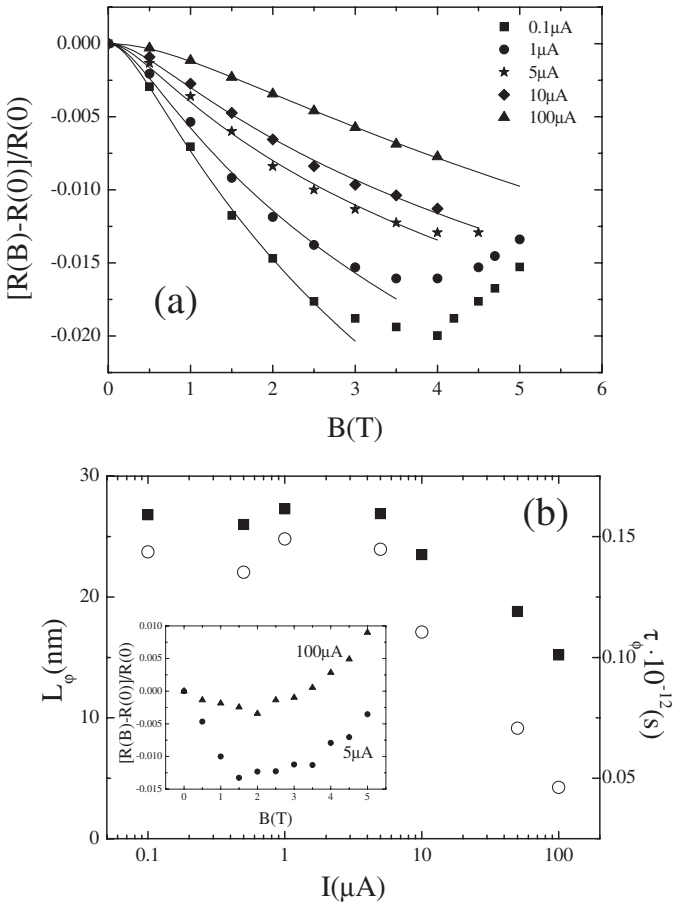


**Fig. 2.** (a) *MR* vs. $B$ for different bias current. The lines are fits to the data using equation (1); (b) inset: *MR* vs. $B$ at different bias current in superfluid $He^4$ bath. Main: fitting parameter of equation (1) $L_\varphi$ (full squares) and $\tau_\varphi$ (empty circles) as a function of the bias current.

and without the external magnetic field respectively, obtained with different dc bias currents at $T = 4.2$ K. The negative *MR* observed below 3 T is indicative of 2D weak localization regime [9] and is given by

$$\frac{R(B) - R(0)}{R(0)} = -R(0)\frac{e^2}{2\pi^2\hbar}\left\{\psi\left(\frac{1}{2} + \frac{\hbar}{4eL_\varphi^2 B}\right) - \ln\left(\frac{\hbar}{4eL_\varphi^2 B}\right)\right\}, \quad (1)$$

where $e$ is the electron charge, $\hbar$ is the Planck constant over $2\pi$, $\Psi$ the di-Gamma function. The data fitting (continuous curves in Fig. 2a) gives a constant value for $L_\varphi = (D\tau_\varphi)^{1/2} = 30$ nm at low bias current with a decrease when the bias current increases above 10 $\mu$A; the typical error bars for the *MR* data in Figure 2a range between one fifth ($\pm 0.001$) and one half ($\pm 0.0025$) of the small ticks spacing. These errors are not relevant for the fittings indeed because we see that the theoretical curves are right on the top of the experimental data. In Figure 2b we report, for each value of the bias current, the values of $L_\varphi$ used for the fit and the corresponding value of $\tau_\varphi$ , obtained assuming $D = 50$ cm$^2$/s [9]. Its value results higher than the elastic scattering time $\tau_0 = 10^{-15}$ s estimated by literature data [9] in agreement with the condition for WL which requires $\tau_\varphi > \tau_0$. This condition is further satisfied if a lower $D$ value is assumed as in the case of semiconductor, bundles and network of SWCNT. At $T = 4.2$ K the condition for *MR* upturn, given by $g\mu_B B/k_B T > 1$ [11] (with $\mu_B$ the Bohr magneton, $g = 2$ the gyromagnetic ratio and $k_B$ the Boltzmann constant), is $B \cong 3$ T, consistent with the experimental result shown in Figure 2a. The dependence of *MR* on the bias current suggests an influence of external electric field on the phase coherence. Possible interpretations based on Joule heating effects can be refused by measuring the sample in a superfluid $^4$He bath. The inset of Figure 2b shows the *MR* vs. $B$ measurements at different bias currents performed on a different sample at $T = 1.7$ K. The very high thermal conductivity

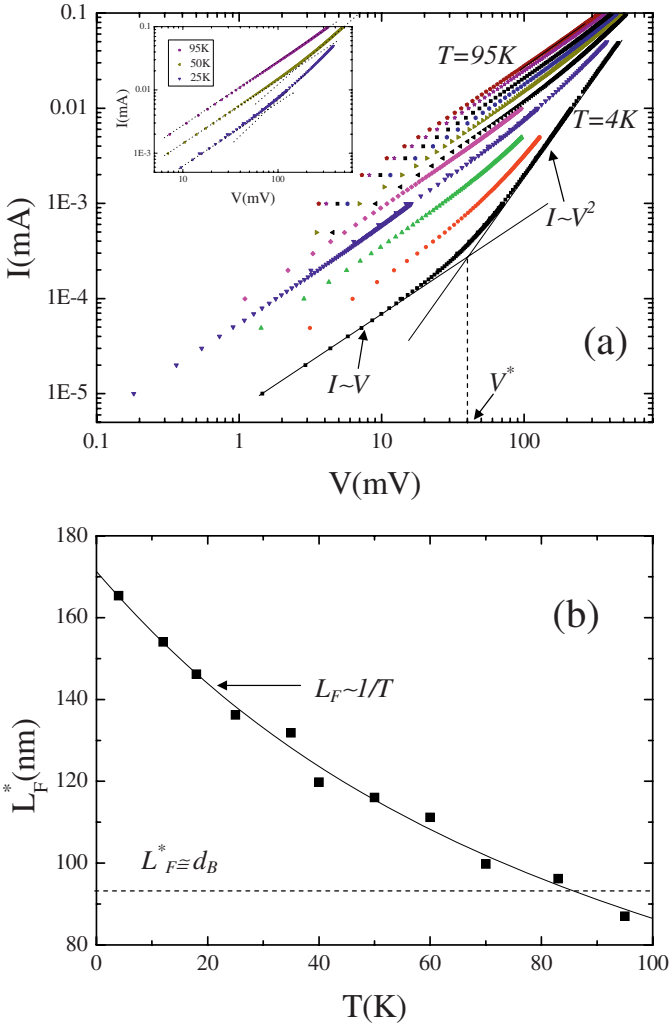


**Fig. 3.** (Color online) $I$-$V$ characteristics at different temperatures. The intersection between the straight lines is representative of the method used for the determination of $V^* = F^* l_c$ in equation (2); inset: three of the $I$-$V$ curves of the main panel clearly showing that the ohmic-non ohmic transition persists at $T = 50$ K and disappears below $T = 95$ K. (b) Temperature dependence of the diffusion length $L_F^*$ obtained from equation (2). The horizontal dashed line is at the value of $L_F^*$ when $T = 85$ K and represents the 2D-3D crossover boundary.

of $^4$He in the superfluid state (He II) would remove all the possible thermal energy generated by Joule heating if it exists. This same qualitative behaviour as that observed in Figure 2a, confirms the external driving force, provided by the electric fields associated with the bias current, as the only cause of the *MR* increase at fixed magnetic field; this phenomenon had been predicted [14], however, evidence of it had not been reported so far.

The effect of an electric field on the localization of electrons was investigated biasing the samples, in zero magnetic field, with a dc current and recording the current-voltage ($I$-$V$) characteristics at different temperatures; the experimental results obtained in this case are shown in Figure 3a. Increasing the current, a transition between an ohmic ($I \sim V$) to a non-ohmic ($I \sim V^2$) regime is clearly observed at low temperature with a crossover voltage $V^*$. Increasing the temperature, $V^*$ increases and the non-ohmic regime is confined at higher current and disappears when $T > 85$ K. A coherence diffusion length is associated to the external electric field $F$ in weak localization regime and is given by [14]:

$$L_F = \left(\frac{\hbar D}{eF}\right)^{1/3}. \tag{2}$$

The substitution of $F^* = V^*/l_c$ inside this expression allows to obtain the temperature dependence of $L_F^*$ which gives the lower limit of the diffusion length for ohmic behaviour. This dependence is reported in Figure 3b where the value $L_F^* = 93$ nm is obtained for $T = 85$ K. This value is of the same order of $d_B$ suggesting that the ohmic-non ohmic transition is strictly connected to the dephasing scattering of the charge carriers wavefunction with the bundle walls when $L_F^* \cong d_B$. The condition $L_F^* \cong d_B$ also characterizes the 2D-3D WL crossover with $T \cong 85$ K the crossover temperature in agreement with data reported by other authors [9,10,15–17]. In Figure 3b we also show that $L_F^*$ follows quite closely a $1/T$ dependence which is represented by the continuous curve in the figure.

This ohmic-non ohmic crossover has been deeply investigated by conductance ($G = 1/R$) vs. $T$ measurements and different bias currents at $B = 0$. Figures 4a and 4b show the experimental data obtained at low current ($I = 0.5$ $\mu$A) and at high current ($I = 100$ $\mu$A) respectively. In both the figures experimental data have been fitted with the theoretical curves obtained for 2D and 3D weak localization theory [6,18]:

$$G_{2D}(T) = G_0 + \frac{e^2}{2\pi^2\hbar}\frac{S}{l}\ln\left[1 + \left(\frac{T}{T_0}\right)^p\right] \tag{3a}$$

$$G_{3D}(T) = G_0 + \frac{e^2}{\pi^3\hbar}\frac{S}{l}\frac{1}{a}T^{p/2}, \tag{3b}$$

where $G_0$ is the zero temperature limit conductance obtained assuming only elastic scattering by impurities, $S$ and $l$ are the surface section and the length of the sample respectively and a temperature dependence of the coherence diffusion length $L_\varphi = aT^{-p/2}$ is assumed.

The value $I = 0.5$ $\mu$A polarizes the sample in the ohmic-non ohmic transition region observed below 85 K in the $I$-$V$ characteristics of Figure 3a. Biasing the sample with $I = 100$ $\mu$A, the ohmic region is explored without any crossing between the two regions. As a result, at low bias the data of Figure 4a are well fitted by the 2D WL curve for temperature below 85 K and with the 3D WL curve for $T > 85$ K. At high bias current, on the other hand, the 3D WL curve represents the best fit of the data over the whole temperature range (4–250 K). Fit procedure using 1D model [6] were unsuccessful with any reasonable value of the fitting parameters. These results are in agreement with the temperature dependence of $L_F^*$ shown in Figure 3b which suggests a 3D regime at high bias when

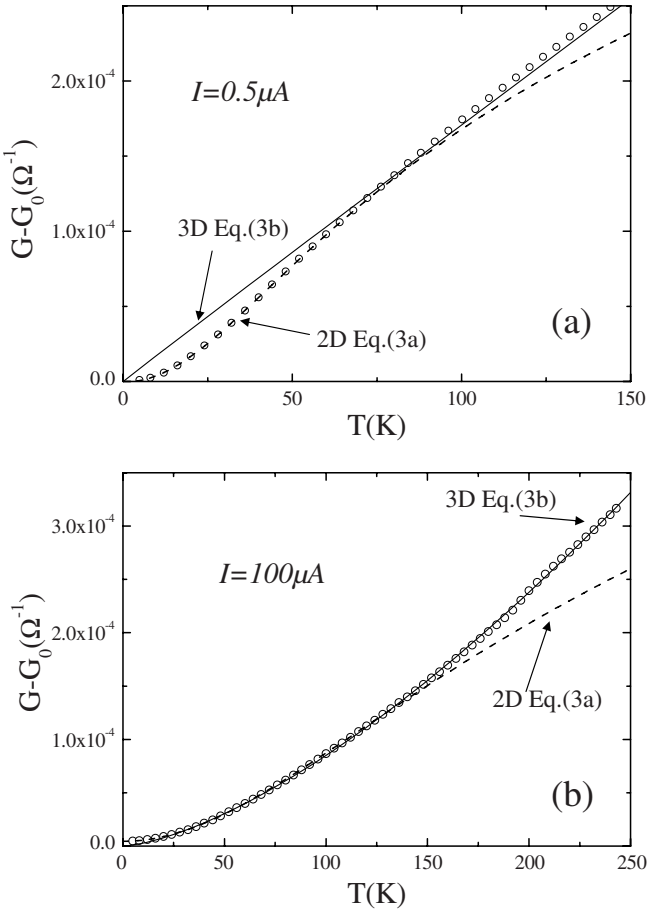


**Fig. 4.** (a) Conductance vs. temperature measurements for $I = 0.5$ $\mu$A. The lines are fit to the data using equations (3a) (dashed line) and (3b) (continuous line) in the range (4−85) K and (85–300) K respectively; (b) same as (a) but with $I =$ 100 $\mu$A and equation (3b) fitting the data in the whole temperature range.

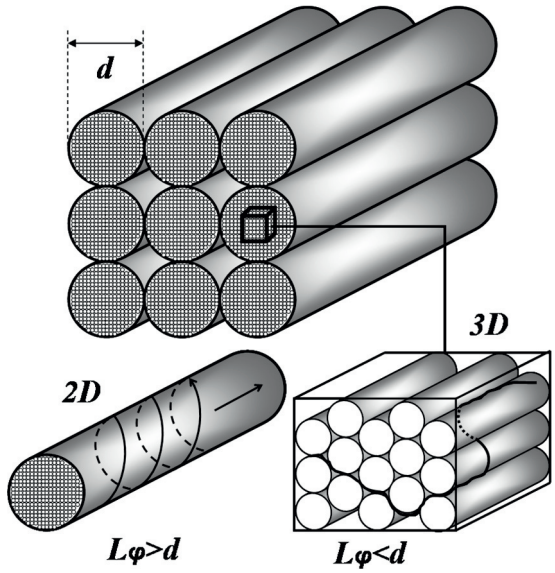


**Fig. 5.** Sketch of our aligned bundles systems illustrating the 2D to 3D transition: the big cylinders on the top picture represent the bundles which are in turn filled with single walled nanotubes. When the phase coherence length is larger than the diameter of the bundles (left) the electron will move only along the bundles axes and on the surface of the bundle (the potential to leave the surface of the bundle is relatively high): only two coordinates are necessary to localize the electrons. Instead, when the phase coherence length is smaller than the size of the bundles (right) the charge carriers are free to move in the direction along the bundles axes and all around a planar section of bundle between the nanotubes (the inter nanotube potential is low). Three coordinates would be necessary to localize the electrons, two on the plane and one for the axis: a typical 3D path is shown in the figure.

$L_F^* < d_B$ and a 2D regime at low bias when $L_F^* > d_B$. The 2D-3D crossover observed in Figure 4a is due to the increasing temperature in an otherwise 2D regime. At high bias, the already established 3D WL regime does not allow any temperature dependence crossover. The exponent $p$ for the 2D model, obtained by the fitting procedure, is $p = 2.12$ which indicates an electron-electron scattering process in the non-ohmic region [11,19,20]. The electron-electron scattering is favoured by the lowering of the dimensionality which increases the interaction probability between the carriers [6,11]. We also note now that the two above expressions (3a) and (3b) are derived under the assumption that the average lifetime for inelastic scattering depends on the temperature according to the relation $\tau_i \propto T^{-p}$. Thus, using $p$ as a fitting parameter for the $G$ vs. $T$ data it is possible to obtain information on inelastic scattering. We have seen that the data of Figure 4a return $p \cong 2$ which is the exponent expected for electron-electron scattering [20]; $L_F^*$ is related to the time by $L_F^* = \sqrt{D\tau_i} \propto T^{-p/2}$ which, for $p = 2$ gives $L_F^* \propto T^{-1}$ in agreement with Figure 3b.

Our data show that the dimensional crossover is governed by $L_F^*$ and takes place when $L_F^* \cong d_B \gg d_{SWCNT}$. This suggests that most of the dissipative processes are due to the bundles-bundles interface in agreement with the hypothesis that the highest potential barriers are localized there [21]. The SWCNT-SWCNT interfaces inside each bundle, on the other side, present a much lower energy barrier which can be crossed by carriers with minor effect on transport properties [22]. When $L_F^* \geq d_B$ the electrons are confined on the bundle surface moving along the tube axis (see the sketch of Fig. 5 on the left part) which is the current bias direction but their wavefunction is expected to be correlated along the tube surface. Any correlation length presents, in this case, two components which are the tube axis direction and the eccentric anomaly angle (2D). Nevertheless, when $d_{SWCNT} < L_F^* < d_B$ electrons move inside the bundles (see Fig. 5 on the right) and the low potential energy interfaces between the inner SWCNT allow a third component of the correlation length along the bundle radius (3D).

In conclusion, within the framework of WL theory we have shown that the phase coherence is affected by external electric field and temperature and we have illustrated how a 2D-3D WL crossover can be induced in

SWCNT bundles aggregates by temperature and bias current variation.

This work has been partially supported by the *GESTO* program of the Regione Lazio, Italy.

## References


1. Y. Imry, *Introduction to Mesoscopic Physics*, 2nd edn. (Oxford Univ. Press, New York, 2002)
2. E. Akkermans, G. Montambaux, *Mesoscopic Physics of Electrons and Photons* (Cambridge Univ. Press, New York, 2007)
3. F.A. Buot, Phys. Rep. **234**, 73 (1993)
4. P. Sheng, B. van Tiggelen, Waves Random Complex Media **17**, 235 (2007)
5. M. Ferrier, A. Kasumov, R. Deblock, S. Guéron, H. Bouchiat, J. Phys. D **43**, 374003 (2010)
6. P.A. Lee, T.V. Ramakrishnan, Rev. Mod. Phys. **57**, 287 (1985)
7. D.E. Beutler, N. Giordano, Phys. Rev. B **38**, 8 (1988)
8. V. Bayot, L. Piraux, J.P. Michenaud, J.P. Issi, Phys. Rev. B **40**, 3514 (1989)
9. S.N. Song, X.K. Wang, R.P.H. Chang, J.B. Ketterson, Phys. Rev. Lett. **72**, 697 (1994)
10. M.S. Fuhrer, W. Holmes, P.L. Richards, P. Delaney, S.G. Louie, A. Zettl, Synth. Met. **103**, 2529 (1999)
11. G. Bergmann, Phys Rep. **107**, 1 (1984)
12. M.L. Terranova et al., J. Phys.: Condens. Matter **19**, 225004 (2007)
13. M. Salvato, M. Cirillo, M. Lucci, S. Orlanducci, I. Ottaviani, M.L. Terranova, F. Toschi, J. Phys. D **45**, 105306 (2012)
14. M. Kaveh, M.J. Uren, R.A. Davies, M. Pepper, J. Phys. C Solid State Phys. **14**, 413 (1981)
15. G. Baumgartner, M. Carrard, L. Zuppiroli, W. Bacsa, W.A. Heer, L. Forrò, Phys. Rev. B **55**, 6704 (1997)
16. M. Baxendale, V.Z. Mordkovich, S. Yoshimura, Phys. Rev. B **56**, 2161 (1997)
17. G.T. Kim, E.S. Choi, D.C. Kim, D.S. Suh, Y.W. Park, Phys. Rev. B **58**, 16064 (1998)
18. L. Langer, V. Bayot, E. Grivei, J.-P. Issi, J.P. Heremans, C.H. Olk, L. Stockman, C. Van Haesendonck, Y. Bruynseraede, Phys. Rev. Lett. **76**, 479 (1996)
19. P.K. Choudhury, M. Jaiswal, R. Menon, Phys. Rev. B **76**, 235432 (2007)
20. N.W. Ashcroft, N.D. Mermin, *Solid State Physics* (Holt Rinehart & Winston, New York, 1976)
21. M. Salvato, M. Cirillo, M. Lucci, S. Orlanducci, I. Ottaviani, M.L. Terranova, F. Toschi, Phys. Rev. Lett. **101**, 246804 (2008)
22. H. Xie, P. Sheng, Phys. Rev. B **79**, 165419 (2009)